Monthly Notices
of the
ROYAL ASTRONOMICAL SOCIETY

MNRAS **518,** 5253–5259 (2023) https://doi.org/10.1093/mnras/stac3335
Advance Access publication 2022 November 28

The galaxy size to halo spin relation of disc galaxies in cosmological hydrodynamical simulations

Hang Yang ,[1,2★] Liang Gao,[1,2,3] Carlos S. Frenk,[3] Robert J. J. Grand ,[4,5,6] Qi Guo,[1,2] Shihong Liao [7] and Shi Shao [3]

[1] *Key Laboratory for Computational Astrophysics, National Astronomical Observatories, Chinese Academy of Sciences, Beijing 100012, China*
[2] *School of Astronomy and Space Science, University of Chinese Academy of Sciences, 19 A Yuquan Rd, Shijingshan District, Beijing 100049, China*
[3] *Institute for Computational Cosmology, Department of Physics, Durham University, Science Laboratories, South Road, Durham DH1 3LE, UK*
[4] *Max-Planck-Institut für Astrophysik, Karl-Schwarzschild-Str 1, D-85748 Garching, Germany*
[5] *Instituto de Astrofísica de Canarias, Calle Vía Láctea, E-38205 La Laguna, Tenerife, Spain*
[6] *Departamento de Astrofísica, Universidad de La Laguna, Av. del Astrofísico Francisco Sánchez, E-38206 La Laguna, Tenerife, Spain*
[7] *Department of Physics, University of Helsinki, Gustaf Hällströmin katu 2, FI-00014 Helsinki, Finland*

Accepted 2022 November 9. Received 2022 November 9; in original form 2021 October 29

ABSTRACT

In the standard disc galaxy formation model, the sizes of galactic discs are tightly related to the spin parameters λ of their dark matter haloes. The model has been wildly adopted by various semi-analytical galaxy formation models which have been extremely successful to interpret a large body of observational data. However, the size–λ correlation was rarely seen in most modern hydrodynamical simulations of galaxy formation. In this short paper, we make use of 4 sets of large hydrodynamical simulations to explore the size–spin parameter relation with a large sample of simulated disc galaxies and compare it with a popular disc galaxy formation model of Mo et al. (1998). Intriguingly, galactic sizes correlate with spin parameters of their dark matter haloes in the simulations developed by the IllustrisTNG collaborations, albeit the relation does not always agree with prediction of MMW98 model overall stellar mass range we examined. There is also a size–spin correlation for the Milky Way analogies in the EAGLE simulations, while it is relatively weaker than that of the IllustrisTNG counterparts. For the dwarfs in the simulations from the EAGLE collaboration, there is NULL correlation. We conclude that either the detailed subgrid physics or hydrodynamics solvers account for the size-spin parameter relation, which will be explored in our future work.

Key words: galaxies: disc – galaxies: formation – galaxies: haloes.

1 INTRODUCTION

In the classic galaxy formation theory (White & Rees 1978; Fall & Efstathiou 1980; White & Frenk 1991), galaxies form in two-stages: dark matter collapse to form self-bound dark matter haloes due to gravitational instability; because of radiative cooling, baryons condense in centres of dark matter haloes to form gaseous disc as a consequence of angular momentum conservation. These cold gas later further fragment and form luminous galaxies when certain conditions are satisfied.

In this framework, since the baryons and dark matter are expected to be initially well mixed and hence experience similar tidal torques (Peebles 1969; White 1984), the galactic disc, which is a consequence of gas condensation, should have similar specific angular momentum as its dark matter halo, namely $j_{\rm d} \sim j_{\rm h}$. Here, $j_{\rm d}$ and $j_{\rm h}$ are specific angular momentum of galaxy and halo, respectively. The specific angular momentum of a dark matter halo $j_{\rm h}$ is often characterized by a dimensionless spin parameter λ (Bullock et al. 2001), which can be written as

$$\lambda = \frac{j_{\rm h}}{\sqrt{2} V_{200} R_{200}}, \quad (1)$$

where R_{200} represents the virial radius of a dark matter halo within which the enclosed mean density is 200 times the critical density of the Universe and M_{200} is the mass enclosed within R_{200}. V_{200} is the virial velocity of the halo, $V_{200} = \sqrt{G M_{200}/R_{200}}$.

Assuming the angular momentum of the stellar disc is a fraction $f_{\rm j} = j_{\rm d}/j_{\rm h}$ of the halo, Mo, Mao & White (1998) (hereafter MMW98) links the size of a disc galaxy $r_{\rm d}$ and virial radius R_{200} of its host dark matter halo with a form as[1]

$$\frac{r_{1/2}}{R_{200}} = \frac{1.68}{\sqrt{2}} f_j f_R \lambda, \quad (2)$$

where the f_R factor is introduced to account for the different rotation velocity curve of the galaxy due both to dark matter adiabatic contraction (Blumenthal et al. 1986) and the self gravitational effects of the disc

The angular momentum-based models (e.g. MMW98) have been successful to explain the observed distribution of disc scale lengths (e.g. Shen et al. 2003; Somerville et al. 2008b; Kravtsov 2013; Huang et al. 2017; Lapi, Salucci & Danese 2018; Posti et al. 2020; Zanisi et al. 2020), and been widely used in various semi-analytical models (e.g. Cole et al. 2000; Hatton et al. 2003; Croton et al. 2006; De

★ E-mail: hyang@nao.cas.cn

[1]Compared with the original MMW98 model, we use a different definition for spin parameter λ. Hence, there is no f_c factor here.

Lucia & Blaizot 2007; Somerville et al. 2008a) by adopting both f_j and f_R to be units. Recent semi-analytical models have been improved by assuming the cooling gas carrying the same specific angular momentum as that of the host halo at each time-step, which later is added to the stellar disc via star formation (e.g. Dutton & van den Bosch 2009; Guo et al. 2011). These semi-analytical models, combined with *N*-body simulations, have been very successful to match a large body of observables, including galaxy size and morphological types, etc. In addition, this improvement makes the model predictions more in line with later studies that the angular momentum vector of the gas and dark matter are not necessary to be identical (e.g. Sharma & Steinmetz 2005; Sales et al. 2009; Liao et al. 2017; Posti et al. 2018; Irodotou et al. 2019).

The formation of disc galaxy has also been extensively investigated with hydrodynamical simulations (e.g. Katz & Gunn 1991; Navarro & White 1994; Steinmetz & Navarro 1999). Until recently, with significant progress in sub-grid physics models, in particularly the feedback model, many modern hydrodynamical galaxy formation simulations are able to reproduce galaxies with different morphological types (e.g. Scannapieco et al. 2012; Dubois et al. 2014; Hirschmann et al. 2014; Vogelsberger et al. 2014; Schaye et al. 2015; Teklu et al. 2015). However, studies based on some of these modern hydrodynamical simulations, suggested that, while sizes of the simulated galaxies are statistically proportional to the virial radius of their host dark matter haloes, there are no correlations between halo spin parameters λ (Ceverino et al. 2014; Wang et al. 2015b; Zolotov et al. 2015; Jiang et al. 2019). This result challenges the classical theory and many existing semi-analytical models. On the contrary, Desmond et al. (2017) found a weak correlation between galaxy size and host halo spin parameter in the EAGLE simulation. Liao et al. (2019) found that there is a strong correlation between sizes and host halo spin parameters λ for field dwarf galaxies in the AURIGA simulation.

In this paper, we use four sets of high-resolution hydrodynamical simulations, to explore the relation between the sizes and spin parameters of host dark matter haloes of a large sample of simulated disc galaxies, and explicitly compare them with predictions from the MMW98. The paper is organized as follows. In Section 2, we briefly introduce the numerical simulations and methodology used in this study. The main results are presented in Section 3, and conclusions are drawn in Section 4.

2 THE SIMULATIONS AND METHODOLOGY

The numerical simulations used in this paper comprise 4 suits of large hydrodynamical galaxy formation simulations, the ILLUSTRISTNG (Sawala et al. 2016), AURIGA (Grand et al. 2017), EAGLE (Crain et al. 2015), and APOSTLE-L2 projects (Sawala et al. 2016). The former two simulations are performed with the same hydrodynamical scheme of the AREPO (Springel 2010) code and with similar subgrid physics models developed by the Illustris collaborations, the latter two are run with the improved smoothed particle hydrodynamics (SPH) and identical subgrid physics model developed by the EAGLE collaborations (Crain et al. 2015).

2.1 The simulations

The ILLUSTRISTNG project (Marinacci et al. 2018; Naiman et al. 2018; Nelson et al. 2018; Springel et al. 2018; Pillepich et al. 2018b) is a suite of cosmological magnetohydrodynamic simulations, which was performed with the magnetohydrodynamic moving mesh code AREPO (Springel 2010). The ILLUSTRISTNG project assume $\Omega_m = 0.3089$, $\Omega_b = 0.0486$, $\Omega_\Lambda = 0.6911$, $h = 0.6774$, $n_s = 0.9667$, and $\sigma_8 = 0.8159$ (Planck Collaboration XVI 2014). In this work, we use the TNG100-1 project with a box size about 110 Mpc. We refer the reader for the detailed galaxy formation models of the ILLUSTRISTNG simulations to Weinberger et al. (2017) and Pillepich et al. (2018a).

Table 1. Numerical parameters of the simulations used in this study. The columns shows: (1) softening length (2) baryonic particles mass; (3) dark matter particles mass.

	ϵ (pc)	m_b ($M_\odot$)	m_{DM} ($M_\odot$)
AURIGA	369	5×10^4	3×10^5
TNG100-1	740	1.4×10^6	7.5×10^6
APOSTLE-L2	216	1.2×10^5	5.8×10^5
EAGLE(RefL0100N1504)	700	1.8×10^6	9.7×10^6

The AURIGA project (Grand et al. 2017) comprises a suite of 30 zoom-in cosmological simulations of Milky Way (MW)-sized haloes and their surroundings. The parent haloes in AURIGA were selected from a dark matter only simulation EAGLE (L100N1504) (Schaye et al. 2015). Similar to the TNG100-1, the AURIGA projects were performed with the magnetohydrodynamic moving mesh code AREPO (Springel 2010), but assume slightly different Cosmological parameters, $\Omega_m = 0.307$, $\Omega_b = 0.048$, $\Omega_\Lambda = 0.693$, $h = 0.6777$, $n_s = 0.9611$, and $\sigma_8 = 0.829$ (Planck Collaboration XVI 2014).

The EAGLE project (Crain et al. 2015; Schaye et al. 2015) is a suite of cosmological hydrodynamic simulations, which were performed with a version of the *N*-body Tree-PM smoothed particle hydrodynamics (SPH) code GADGET-3 by Springel, Di Matteo & Hernquist (2005). The cosmological parameters adopted in the EAGLE project are $\Omega_m = 0.307$, $\Omega_b = 0.048$, $\Omega_\Lambda = 0.693$, $h = 0.6777$, $n_s = 0.9611$, and $\sigma_8 = 0.829$ (Planck Collaboration XVI 2014). In this work, we use the Ref-L0100N1504 run which has a volume of $(100\,\mathrm{Mpc})^3$.

The APOSTLE project (Fattahi et al. 2016; Sawala et al. 2016) performed a suite of cosmological hydrodynamic zoom-in simulations of 12 volumes selected to match the kinematics of Local Group. High-resolution regions of the APOSTLE were selected from dark matter only simulation DOVE which evolved a cosmological volume of $(100\,\mathrm{Mpc})^3$. The APOSTLE project was performed with the same code GADGET-3 as EAGLE, and run with three different resolutions: low(L1), medium(L2), and high(L3). Since only two volumes have been run at high-resolution (L3) in APOSTLE, we use the medium-resolution (L2) data in this work. The cosmological parameters in APOSTLE simulation adopt the result of WMAP-7, namely $\Omega_m = 0.272$, $\Omega_b = 0.0455$, $\Omega_\Lambda = 0.728$, $h = 0.704$, $n_s = 0.967$, and $\sigma_8 = 0.81$ (Komatsu et al. 2011).

The Table 1 summarize the typical individual particle mass and softening length for all the above simulations.

In all the above simulations, dark matter haloes are identified with friends-of-friends (FoF) algorithm (Davis et al. 1985) and subhaloes are subsequently identified with the SUBFIND algorithm (Springel et al. 2001; Dolag et al. 2009).

2.2 Determination of galaxy morphology and halo spin parameter

In order to reliably measure the sizes of the simulated galaxies, we include all central galaxies containing at least 250[2] stellar

[2]We have also selected galaxies that have at least 1000 stellar particles (Tacchella et al. 2019) and found the result remains are qualitatively similar.

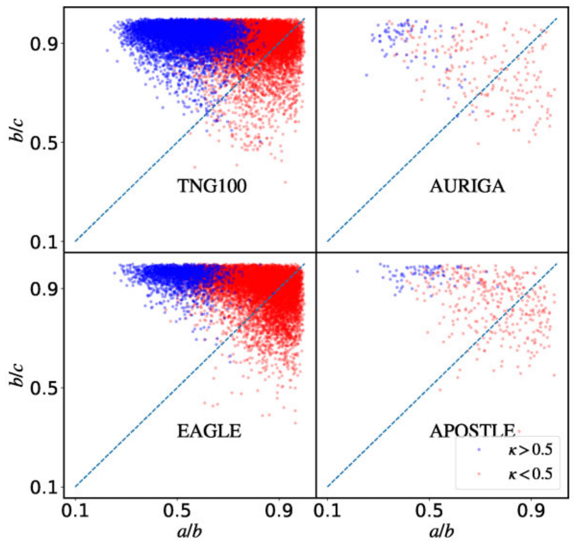

Figure 1. Axial ratio *b*/*c* verus *a*/*b* of each simulated galaxy in our sample. The blue dots represent disc-like galaxies, the red dots represent spheroidal-like galaxies, and the blue dash lines in each panel indicate $b/c = a/b$ ($b/c > a/b$ for oblate, $b/c < a/b$ for prolate).

particles and host halo mass satisfy $\log(M_{200}/\mathrm{M}_\odot) < 12.3$. These galaxies span almost four orders of magnitude in stellar mass and reside in a variety of environments. We further discard the galaxies contaminated by low-resolution particles in the zoom-in AURIGA and APOSTLE simulations. We have excluded all the satellites but only use the central galaxies in this study. The final galaxy sample contains 19 315 galaxies from the TNG100-1, 282 galaxies from the AURIGA, 12 327 galaxies from the EAGLE, and 408 galaxies from the APOSTLE.

We define the morphology of each galaxy of the above galaxy sample by introducing the κ parameter defined as the ratio of rotational kinetic energy $K_{\rm rot}$ to total kinetic energy K for a galaxy (Sales et al. 2012), written as

$$\kappa = \frac{K_{\rm rot}}{K} = \frac{\sum_i 1/2m_i\{(\hat{\boldsymbol{L}} \times \hat{\boldsymbol{r}}_i)\cdot \boldsymbol{v}_i\}^2}{\sum_i 1/2m_i v_i^2}, \quad (3)$$

Where $\hat{\boldsymbol{L}}$ is the unity total angular momentum vector of stellar components. The m_i, r_i, and v_i are mass, position vector to centre, velocity vector to centre for stellar particle i, respectively.

For each galaxy in our sample, we calculate its κ parameter with all star particles within 2 times of its half-stellar-mass radius, $2r_{1/2}$. A galaxy is classified as a disc (or spheroidal) galaxy if its $\kappa > (<) 0.5$. Note, κ is a definition of morphology according to kinematics and correlates strongly with the axial ratios of a galaxy. In Fig. 1, we show *b*/*c* versus *a*/*b* of our galaxy sample in different simulations. Here the axial ratios of galaxies are obtained by diagonalizing the inertia tensor matrix,

$$I_{\alpha\beta} = \Sigma_i m_i (x_{i,\alpha} - x_{c,\alpha})(x_{i,\beta} - x_{c,\beta}), \quad (4)$$

where x_i is the spatial position for particle i and x_c is the position with the minimal gravitational potential for the galaxy. We calculate the inertia matrix by the stellar components within twice the stellar half-mass radius, $a < b < c$ are eigenvalues of the inertia tensor matrix $I_{\alpha\beta}$.

The disc galaxies are shown as blue dots and spheroidal galaxies are shown as red ones. As can be seen clearly that the classification of galaxy morphology type with $\kappa = 0.5$ is reasonable. We also tested other critical values for κ(from 0.4 to 0.5), and it had little effect on the final correlation results. We summarize the number of various samples in the Table 2. It is worth noting that our kinematic morphological classification differs from the standard photometry-based method used in observation, with the two showing a moderate correlation with considerable scatter (e.g. Abadi et al. 2003; Scannapieco et al. 2010).

Table 2. Sample number of the simulations used in this study. The columns shows: (1) total sample number (2) disc galaxies number($\kappa > 0.5$); (3) spheroidal galaxies number($\kappa < 0.5$).

	All	Disc	Spheroidal
AURIGA	282	77	205
TNG100-1	19 315	6615	12 700
APOSTLE-L2	408	71	337
EAGLE(RefL0100N1504)	12 327	1831	10 496

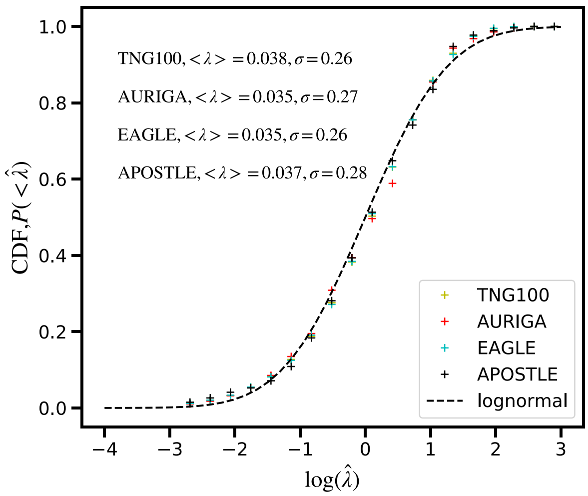

Figure 2. Cumulative distribution of normalization spin parameter $\hat{\lambda} = (\log_{10}\lambda - <\log_{10}\lambda>)/\sigma$ of all dark matter halo samples in different simulations. Results from different simulations are shown in different colors as indicated on the label. The dashed lines show a standard single log-normal distribution. Mean values and standard deviation of spin parameters of different simulations are also shown in the figure.

For each halo in our sample, we calculate its dimensionless spin parameter λ using the formula given by (Bullock et al. 2001).

$$\lambda = \frac{j_{\rm h}(< R_{200})}{\sqrt{2}V_{200}R_{200}} \quad (5)$$

Previous works have shown that the distribution of halo spin parameter λ is independent of halo mass and follow a log-normal distribution with the mean value $<\lambda> \sim 0.03$–0.04 and standard deviation $\sigma_{\log_{10}\lambda} \sim 0.2$–$0.3$ (Bett et al. 2007; Macciò et al. 2007; Jiang et al. 2019). In Fig. 2, we show the cumulative halo spin parameter distributions of our halo sample of all simulations used in this study without morphology cut, results for different simulations are distinguished with different colors as indicated in the label. Mean values and standard deviation of spin parameters of different simulations are also shown on the label. Clearly, these results are consistent with each other and with previous works.

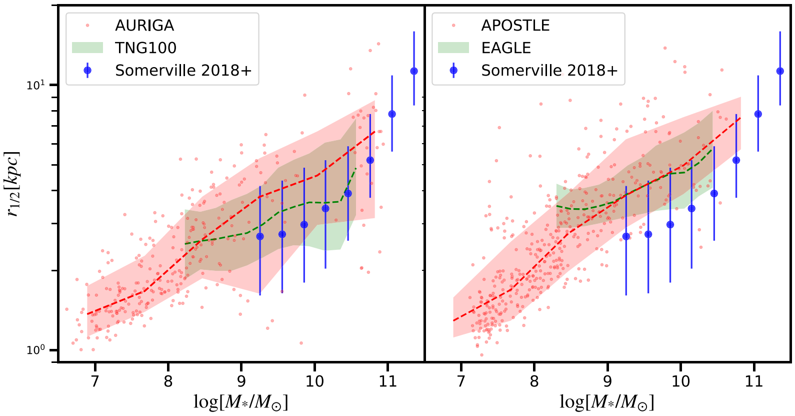

Figure 3. Galaxy size–mass relation in different simulations (*left-hand panel*: AURIGA and TNG100-1 simulations; *right-hand panel*: APOSTLE and EAGLE simulations) at $z = 0$. Shaded regions show 16th to 84th percentiles of the result in each stellar mass bin. The thick blue points show the observed relation by Somerville et al. (2018), and error bars show 1σ scatter.

3 RESULTS

3.1 Galaxy size–stellar mass relations

Compared with observations, we adopt a different morphology definition method (κ) here. In Fig. 3, we present the size–stellar mass relation of all simulated galaxies at $z = 0$ without morphology cutting, and then fairly compare the results with observations. The results for the AURIGA and TNG100-1 are shown in the left-hand panel and those for the APOSTLE and EAGLE are shown in the right-hand panel, results for different simulations are distinguished with different colours as shown in the label. The shaded areas show 1σ scatters of each simulation, and the median values are shown with dashed lines. Here, the size of a simulated galaxy is defined as the half-mass radius within which the enclosed stellar mass is half of the whole galaxy. In all simulations, galaxy sizes increase with increasing galaxy stellar masses with $r_{1/2} \sim 1$ kpc for low-mass dwarf galaxies, and $r_{1/2} \sim 5$ kpc for MW-mass galaxies. We find overall a good agreement between the full-box simulations (TNG100-1 and EAGLE) and their zoom-in counterparts (AURIGA and APOSTLE) at the mass where the two simulations overlap. For masses $M_\star \leq 10^{10.5}$ $M_\odot$, the size–mass relation of the galaxies in TNG100-1 and EAGLE is almost flat, while the slope of the zoom-in galaxies in APOSTLE or AURIGA is much steeper, the small difference in the slope is due to the effect of simulation resolution on the size of the galaxies as studied in prior literature (e.g. Pillepich et al. 2018b; Ludlow et al. 2019).

We then compare the size–mass relations of simulated galaxies with an observational study by Somerville et al. (2018) (blue dots with error bars). The conversion of the observational projected semimajor half-light radius $r_{e,\,2d}$ into $r_{1/2}$ involves two factors,

$$r_{e,2d} = f_p f_k r_{1/2}. \quad (6)$$

The projection correction factor $f_p = 1(0.68)$ and the light to mass weighting factor $f_k = 1.2(1.15)$ for disc (spheroidal) galaxies in Somerville et al. (2018). The observational results clearly also show an increasing slope for galaxies with stellar mass. At masses, $M_\star \geq 10^{9.5}$ $M_\odot$, the agreement between TNG100-1 and observations is rather good (see the left-hand panel in Fig. 3), consistent with the study by Genel et al. (2018). AURIGA uses the same hydrodynamics solver and similar subgrid physics with TNG100-1. Thus, the sizes of AURIGA central galaxies that have stellar mass, $M_\star \geq 10^{10.5}$ $M_\odot$, also agree with the observations.

For galaxies in EAGLE and APOSTLE (right-hand panel in Fig. 3), the sizes are systematically about 0.17 dex larger than the observed values, whereas Furlong et al. (2017) who uses the same EAGLE data found a better agreement with observation than our result. The discrepancy could be due to the fact that Furlong et al. (2017) selected galaxies in a redshift bin of $\Delta z = 0.5$ while we only make use of galaxies at $z = 0$, and the inclusion of high-redshift galaxies could reduce the median of the galaxy sizes. A secondary effect is a different definition of disc galaxies. The final effect is that our definition of size $r_{1/2}$ is typically larger than if we take into account the stellar particles within a specific spherical aperture. Furlong et al. (2017) adopted an aperture of radius, $r = 100$ kpc, to exclude the stellar particles that belong to the galaxy by the subhalo but are located far out. However, the aperture measurements only affect very high mass galaxies with $M_\star \geq 10^{10.5}$ $M_\odot$ which is larger than most of our selected galaxies. In addition, the results for passive and active galaxies were separated when Furlong compared EAGLE with observations.

3.2 Galactic size–host halo spin parameter relations

In Fig. 4, we show $r_{1/2}/R_{200}$ of each simulated galaxy ($\kappa > 0.5$) of our sample versus spin parameter λ of its host halo. The upper panels show results for MW-sized galaxies and the bottom show results for dwarfs, results from different simulations are shown with different symbols as indicated in the label. Here, we follow (e.g. Wang et al. 2015a, 2020) to define MW-sized galaxies as the galaxies whose halo masses are in the range, $M_{200} \in [0.5, 2] \times 10^{12}$ $M_\odot$, and dwarfs as those with halo masses ranging from $M_{200} \lesssim 1.5 \times 10^{11}$ $M_\odot$. The thick black dots indicate the median values of each λ bin in the TNG100-1 and EAGLE simulations. Error bars show the 16th–84th percentile of the size ratios. There is a strong correlation between the $r_{1/2}/R_{200}$ and λ for $\lambda \geq 0.01$ in the TNG100-1 and AURIGA, while there is very weak or no correlation below the value. Interestingly, the λ–size relation is much weaker in the EAGLE and APOSTLE simulations. Table 3 summarizes the values of the Spearman correlation coefficient ρ_s of all simulations.

The purple and blue dashed lines in all panels show predictions of Mo et al. (1998) models, assuming $f_j = 1$ and $f_j = 0.5$, respectively. Interestingly, MMW98 model with $f_j = 0.5$ agrees reasonably with TNG100-1 and AURIGA for the MWs samples, while the agreement is worse for dwarfs, even though the AURIGA dwarfs seems to agree with MMW98 with $f_j = 1$. It is noticeable that the $r_{1/2}/R_{200}$ of the AURIGA

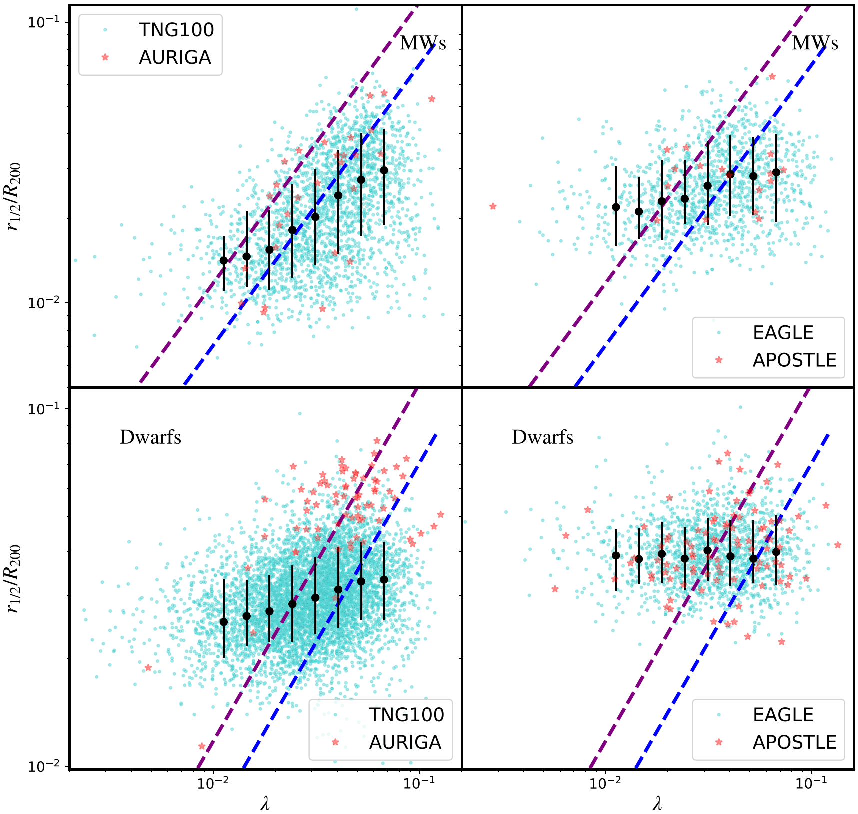

Figure 4. Galaxy $r_{1/2}/R_{200}$ versus host halo spin λ of disc galaxies in our galaxy sample. Black dots show median values of the TNG100 (left-hand panels) or Eagle (right-hand panels) disc galaxies, respectively. Error bars show 16th and 84th percentiles in each λ bin. The dashed line display predictions given by the MMW98 model assuming $f_j = 1.0$ (purple) and $f_j = 0.5$ (blue) with $f_R = 1$, respectively.

Table 3. Spearman correlation coefficients ρ for λ–$r_{1/2}/R_{200}$ relation of simulated disc galaxies. Error bars are estimated with Fisher transformation method assuming 95 per cent confidence.

	MW-like	Dwarf
ρ(TNG100&Auriga)	0.50 ± 0.05	0.38 ± 0.05
ρ(Eagle&Apostle)	0.32 ± 0.07	0.02 ± 0.09

disc dwarfs tends to be overall larger than those of the TNG100-1. The reason may be due to that the size of AURIGA sample is smaller than the TNG100-1. For dwarf-sized dark matter haloes in the EAGLE and APOSTLE, the size–λ relation is almost null. We have to note that the slope and amplitude of the size–λ relation may also rely on the halo concentration and angular momentum retention factor f_j (see appendix A and B, respectively). Galaxies with lower concentration have larger size in MW-mass sample and galaxies with higher f_j have larger size in all sample.

4 DISCUSSIONS AND CONCLUSIONS

In the classic picture of the disc galaxy formation model, the sizes of disc galaxies are tightly related to the spin parameter of their dark matter haloes. In this short paper, we make use of four sets of modern hydrodynamic simulations of galaxy formation to examine this scenario, and compare results of the simulations with a popular disc galaxy formation model of MMW98. Our results can be summarized as follows.

Galaxy size–stellar mass relations in the IllustrisTNG and EAGLE simulations agree reasonably with observational results, while the agreement is better in the Illustris TNG100; the relation seems convergent in both sets we used, of the Illustris and EAGLE. For the simulated disc galaxies selected with κ, there are moderate correlation between size ratio, $r_{1/2}/R_{200}$, and spin parameter, λ, of dark matter halo in the Illustris family runs, TNG100-1 and AURIGA, while the correlation is weak or null in the EAGLE and APOSTLE simulations. The scatter of the $r_{1/2}/R_{200}$–λ relation could be due to the variety in the halo concentration and retention factor f_j. The spearman correlation coefficient is 0.50 (0.38) for the MW-sized disc galaxies in the Illustris family (EAGLE family), and 0.32 (0.02) for the disc dwarfs in the Illustris family (EAGLE family). The size–spin parameter relation of the simulated MWs in the TNG100-1 and AURIGA simulations agree well with MMW98 model by assuming $f_j = 0.5$, but not for the dwarfs which have different logarithmic slopes from the prediction of the same model.

Intriguingly, on the classic disc formation model, the results from the Illustris and EAGLE family runs are nearly opposite. While the Illustris runs are in qualitatively support of the model, the EAGLE runs, along with an existing study from NIHAO simulation (Jiang et al. 2019), are largely against it. As the hydrodynamic solvers and detailed subgrid physics implemented in different galaxy formation models discussed here are quite different, it is unclear what is the dominant factor to set up the halo spin and stellar disc–size relation seen in the Illustris runs. A pioneering work has shown that EAGLE and AURIGA exhibit different gas properties in the MW-mass galaxies, baryon cycle is almost closed in the AURIGA main galaxy while less baryons reside within the halo in EAGLE (Kelly et al. 2022). We may speculate that baryons may be more tightly related to their dark matter halo in the AURIGA than EAGLE, and thus we see a stronger correlation between galaxy size and halo spin relation in the AURIGA simulation than in EAGLE. Whether this speculation is true and how the detailed feedback physics operates, we will explore in a future study.

ACKNOWLEDGEMENTS

We are grateful to Simon White and Volker Springel for useful discussions. We acknowledge support from NSFC grants (nos 11988101, 11133003, 11425312, 12033008, 11622325, and 11903043), National Key Program for Science and Technology Research Development (2018YFA0404503 and 2017YFB0203300), and K. C. Wong Foundation. LG thanks the hospitality of the Institute for Computational Cosmology, Durham University. CSF acknowledges support by the European Research Council (ERC) through Advanced Investigator DMIDAS (GA 786910). QG acknowledge support from NO. CMS-CSST-2021-A07. RG acknowledges financial support from the Spanish Ministry of Science and Innovation (MICINN) through the Spanish State Research Agency, under the Severo Ochoa Program 2020-2023 (CEX2019-000920-S). SL acknowledges the support by the European Research Council via ERC Consolidator Grant KETJU (No. 818930). QG and SS acknowledge the support from CAS Project for Young Scientists in Basic Research, Grant No. YSBR-062. SS acknowledges the science research grants from the China Manned Space Project with NO. CMS-CSST-2021-B03.

DATA AVAILABILITY

The IllustrisTNG simulations, including the TNG100-1 used in this article, are publicly available and accessible at https://www.tng-project.org/data/. The EAGLE simulation is publicly available at http://eagle.strw.leidenuniv.nl (see McAlpine et al. (2016) for the original data release description). The other data directly related to this publication and its figures is available on request from the corresponding author.

REFERENCES

Abadi M. G., Navarro J. F., Steinmetz M., Eke V. R., 2003, ApJ, 597, 21
Bett P., Eke V., Frenk C. S., Jenkins A., Helly J., Navarro J., 2007, MNRAS, 376, 215
Blumenthal G. R., Faber S. M., Flores R., Primack J. R., 1986, ApJ, 301, 27
Bullock J. S., Kolatt T. S., Sigad Y., Somerville R. S., Kravtsov A. V., Klypin A. A., Primack J. R., Dekel A., 2001, MNRAS, 321, 559
Ceverino D., Klypin A., Klimek E. S., Trujillo-Gomez S., Churchill C. W., Primack J., Dekel A., 2014, MNRAS, 442, 1545
Cole S., Lacey C. G., Baugh C. M., Frenk C. S., 2000, MNRAS, 319, 168
Crain R. A. et al., 2015, MNRAS, 450, 1937
Croton D. J. et al., 2006, MNRAS, 365, 11
Davis M., Efstathiou G., Frenk C. S., White S. D. M., 1985, ApJ, 292, 371
De Lucia G., Blaizot J., 2007, MNRAS, 375, 2
Desmond H., Mao Y.-Y., Wechsler R. H., Crain R. A., Schaye J., 2017, MNRAS, 471, L11
Dolag K., Borgani S., Murante G., Springel V., 2009, MNRAS, 399, 497
Dubois Y. et al., 2014, MNRAS, 444, 1453
Dutton A. A., van den Bosch F. C., 2009, MNRAS, 396, 141
Fall S. M., Efstathiou G., 1980, MNRAS, 193, 189
Fattahi A. et al., 2016, MNRAS, 457, 844
Furlong M. et al., 2017, MNRAS, 465, 722
Genel S. et al., 2018, MNRAS, 474, 3976
Grand R. J. J. et al., 2017, MNRAS, 467, 179
Guo Q. et al., 2011, MNRAS, 413, 101
Hatton S., Devriendt J. E. G., Ninin S., Bouchet F. R., Guiderdoni B., Vibert D., 2003, MNRAS, 343, 75
Hirschmann M., Dolag K., Saro A., Bachmann L., Borgani S., Burkert A., 2014, MNRAS, 442, 2304
Huang K.-H. et al., 2017, ApJ, 838, 6
Irodotou D., Thomas P. A., Henriques B. M., Sargent M. T., Hislop J. M., 2019, MNRAS, 489, 3609
Jiang F. et al., 2019, MNRAS, 488, 4801
Katz N., Gunn J. E., 1991, ApJ, 377, 365
Kelly A. J., Jenkins A., Deason A., Fattahi A., Grand R. J. J., Pakmor R., Springel V., Frenk C. S., 2022, MNRAS, 514, 3113
Komatsu E. et al., 2011, ApJS, 192, 18
Kravtsov A. V., 2013, ApJ, 764, L31
Lapi A., Salucci P., Danese L., 2018, ApJ, 859, 2
Liao S., Gao L., Frenk C. S., Guo Q., Wang J., 2017, MNRAS, 470, 2262
Liao S. et al., 2019, MNRAS, 490, 5182
Ludlow A. D., Schaye J., Schaller M., Richings J., 2019, MNRAS, 488, L123
Macciò A. V., Dutton A. A., van den Bosch F. C., Moore B., Potter D., Stadel J., 2007, MNRAS, 378, 55
Marinacci F. et al., 2018, MNRAS, 480, 5113
McAlpine S. et al., 2016, Astron. Comput., 15, 72
Mo H. J., Mao S., White S. D. M., 1998, MNRAS, 295, 319
Naiman J. P. et al., 2018, MNRAS, 477, 1206
Navarro J. F., White S. D. M., 1994, MNRAS, 267, 401
Nelson D. et al., 2018, MNRAS, 475, 624
Peebles P. J. E., 1969, ApJ, 155, 393
Pillepich A. et al., 2018a, MNRAS, 473, 4077
Pillepich A. et al., 2018b, MNRAS, 475, 648
Planck Collaboration XVI, 2014, A&A, 571, A16
Posti L., Pezzulli G., Fraternali F., Di Teodoro E. M., 2018, MNRAS, 475, 232
Posti L., Famaey B., Pezzulli G., Fraternali F., Ibata R., Marasco A., 2020, A&A, 644, A76
Sales L. V., Navarro J. F., Schaye J., Dalla Vecchia C., Springel V., Haas M. R., Helmi A., 2009, MNRAS, 399, L64
Sales L. V., Navarro J. F., Theuns T., Schaye J., White S. D. M., Frenk C. S., Crain R. A., Dalla Vecchia C., 2012, MNRAS, 423, 1544
Sawala T. et al., 2016, MNRAS, 457, 1931
Scannapieco C., Gadotti D. A., Jonsson P., White S. D. M., 2010, MNRAS, 407, L41
Scannapieco C. et al., 2012, MNRAS, 423, 1726
Schaye J. et al., 2015, MNRAS, 446, 521
Sharma S., Steinmetz M., 2005, ApJ, 628, 21
Shen S., Mo H. J., White S. D. M., Blanton M. R., Kauffmann G., Voges W., Brinkmann J., Csabai I., 2003, MNRAS, 343, 978
Somerville R. S., Hopkins P. F., Cox T. J., Robertson B. E., Hernquist L., 2008a, MNRAS, 391, 481
Somerville R. S. et al., 2008b, ApJ, 672, 776
Somerville R. S. et al., 2018, MNRAS, 473, 2714
Springel V., 2010, MNRAS, 401, 791
Springel V., White S. D. M., Tormen G., Kauffmann G., 2001, MNRAS, 328, 726
Springel V., Di Matteo T., Hernquist L., 2005, MNRAS, 361, 776
Springel V. et al., 2018, MNRAS, 475, 676
Steinmetz M., Navarro J. F., 1999, ApJ, 513, 555
Tacchella S. et al., 2019, MNRAS, 487, 5416
Teklu A. F., Remus R.-S., Dolag K., Beck A. M., Burkert A., Schmidt A. S., Schulze F., Steinborn L. K., 2015, ApJ, 812, 29
Vogelsberger M. et al., 2014, MNRAS, 444, 1518
Wang W., Han J., Cooper A. P., Cole S., Frenk C., Lowing B., 2015a, MNRAS, 453, 377
Wang L., Dutton A. A., Stinson G. S., Macciò A. V., Penzo C., Kang X., Keller B. W., Wadsley J., 2015b, MNRAS, 454, 83

Wang W., Han J., Cautun M., Li Z., Ishigaki M. N., 2020, Sci. China Phys. Mech. Astron., 63, 109801
Weinberger R. et al., 2017, MNRAS, 465, 3291
White S. D. M., 1984, ApJ, 286, 38
White S. D. M., Frenk C. S., 1991, ApJ, 379, 52
White S. D. M., Rees M. J., 1978, MNRAS, 183, 341
Zanisi L. et al., 2020, MNRAS, 492, 1671
Zolotov A. et al., 2015, MNRAS, 450, 2327

APPENDIX A: THE DEPENDENCE OF CONCENTRATION ON SIZE–SPIN RELATION

We use $c \equiv V_{\rm max}/V_{200}$ to explore the dependence of $r_{1/2}/R_{200}$–λ relation on the concentration of the halo. The red (blue) dots in Fig. A1 represent two populations of haloes whose concentration are in the top or bottom 30 per cent of the full sample. For the MW-mass galaxies (top panels), the $r_{1/2}/R_{200}$–λ relations between the two subsets are almost identical in the slope but only differ in the amplitude, with the sizes in low-concentrated samples being 1.4(1.2) times larger than those in high-concentrated samples in IllustrisTNG (EAGLE). Thus, for high-mass galaxies, the size of a galaxy relies on both λ and concentration. However, for dwarf-mass galaxies (bottom panels), the $r_{1/2}/R_{200}$–λ relation between the two samples is very similar, which suggests that for low-mass galaxies the size is mainly determined by λ.

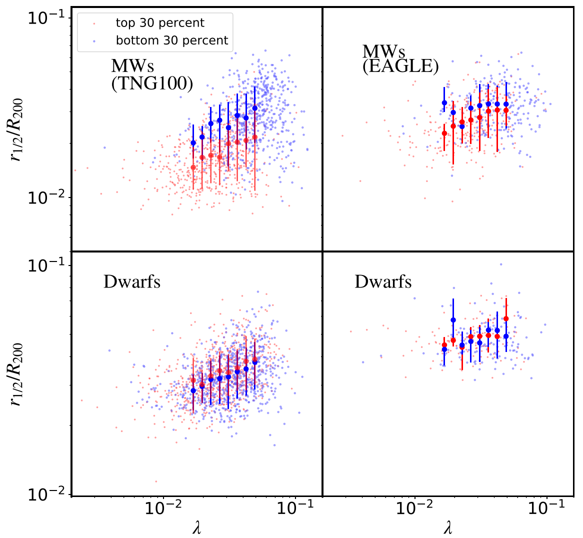

Figure A1. $r_{1/2}/R_{200}$–λ relation of MWs (top panels) and disc dwarfs (bottom panels) in IllustrisTNG (left-hand panels) and EAGLE (right-hand panels). The red and blue dots represent large and small concentration samples, respectively. The thick points and error bars show median value and 1σ scatter for the corresponding samples.

APPENDIX B: THE DEPENDENCE OF ANGULAR MOMENTUM RETENTION FACTOR ON SIZE–SPIN RELATION

Fig. B1 shows the dependence of the scatter of $r_{1/2}/R_{200}$–λ relation on the angular momentum retention factor $f_j = j_d/j_h$. The red (blue) dots represent the populations whose f_j are in the top (bottom) 30 per cent of the full sample. The segregation between the two samples is highly significant, which indicates that $f_j = j_d/j_h$ is responsible for the scatter in the $r_{1/2}/R_{200}$–λ relation.

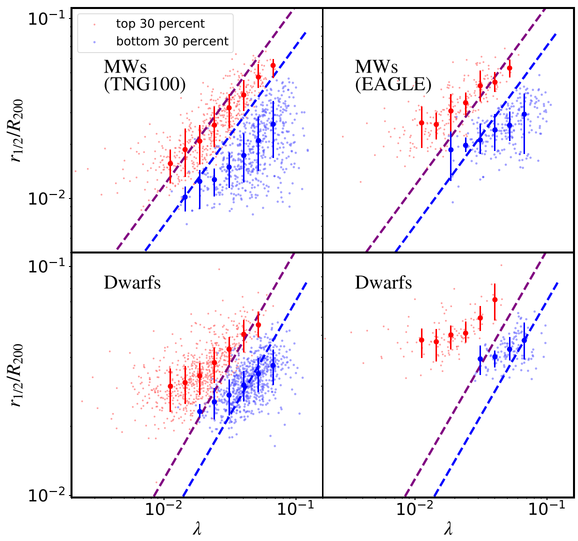

Figure B1. $r_{1/2}/R_{200}$–λ relation of MW (top panels) and dwarf analogues (bottom panels) in IllustrisTNG (left-hand panels) and EAGLE (right-hand panels). The red and blue dots represent the top 30 and bottom 30 per cent of the samples according to their angular momentum retention factor f_j samples, respectively. The thick points and error bars show median value and 1σ scatter for the corresponding samples. The dashed line display predictions given by the MMW98 model assuming $f_j = 1.0$ (purple) and $f_j = 0.5$ (blue) with $f_R = 1$, respectively.

This paper has been typeset from a TEX/LATEX file prepared by the author.